

# Validation of a Novel OpenFOAM Solver using a Supersonic, Non-reacting Channel Flow

Nils C. Dröske\*, Paul Nizenkov†, Jiby J. Vellaramkalayil‡ and Jens von Wolfersdorf§  
*Universität Stuttgart, Institute of Aerospace Thermodynamics (ITLR), 70569 Stuttgart, Germany*

Konrad Makowka\* and Thomas Sattelmayer§

*Technische Universität München, Institute for Thermodynamics, 85748 Garching, Germany*

A newly developed numerical solver for supersonic flow is validated using a non-reacting, hot gas channel flow. The solver is embedded into the open-source software package OpenFOAM, thus allowing massive code parallelization. It uses a transient approach and includes the support of multi-species transport and chemical reactions. A local time stepping technique is applied to remedy the effects of the acoustic Courant number restriction and to speed up convergence. The evaluation is conducted using both experimental data and numerical results of a commercial CFD code. Different flow Mach numbers and wall resolution techniques are evaluated and compared. Two- and three-dimensional simulations with the new solver are shown to provide quasi-steady-state solutions which are comparable to those of the commercial code. In addition to the investigation of the hot gas channel flow Schlieren images obtained for cold flow conditions are compared to the numerically predicted flow field and good agreement is demonstrated. The presented work provides a supersonic channel flow test case, which establishes the basis for further enhancement of our newly created solver.

## Nomenclature

$B$	channel width
$c$	speed of sound
$C$	Courant number
$f$	focal length
$H$	channel height
$\dot{m}$	mass flux
$M$	Mach number
$p$	pressure
$r$	recovery factor
$t$	time
$T$	temperature
$u$	velocity
$u_\tau$	shear velocity

### Subscripts

0	stagnation conditions
$e$	boundary layer edge
$t$	turbulent
$w$	wall

\*Dipl.-Ing., Research Associate, AIAA Student Member

†Dipl.-Ing., currently Research Associate at the Institute of Space Systems, Universität Stuttgart, AIAA Student Member

‡Dr.-Ing.

§Dr.-Ing., Professor

### Symbols

$\gamma$	heat capacity ratio
$\kappa$	von Kármán's constant
$\mu$	dynamic viscosity
$\nu$	kinematic viscosity

## I. Introduction

WHEN designing future aircraft or space transportation systems operating in a high Mach number regime, air breathing engines are an alternative to the commonly used rocket propulsion systems. One of the most promising concepts is the so-called supersonic combustion ramjet, in short scramjet. Within a scramjet engine the flow stays supersonic during the combustion phase, thus reducing pressure losses and enabling higher flight Mach numbers compared to ramjets. Another advantage of this type of propulsion system is the possibility to use the oxidizer provided by the atmosphere instead of carrying it on board. Thereby the maximum payload can be increased significantly while at the same time reducing operational costs. However, due to the high enthalpy flow environment various technical challenges arise.

As it is difficult to obtain high temperature steady state supersonic flow conditions in experimental test beds, numerical simulations are inevitable. As commercial computational fluid dynamics (CFD) software is strongly limited in terms of code modification and also costly if massive parallelization is required, we designed a new solver for compressible multi-species and chemically reacting flows. It is integrated into the open source CFD library OpenFOAM.<sup>1</sup> At first this solver is being validated for a non-reacting channel flow with fuel injectors. For this purpose two-dimensional and three-dimensional cases for different flow Mach numbers have been investigated. A vast experimental and numerical database, which has been established at the Institute of Aerospace Thermodynamics (ITLR),<sup>2-5</sup> was used to validate the new solver. Our numerical simulations showed good agreement to the available data, making the newly developed solver suitable for the application to more geometrically complex and also to reacting supersonic flows.

## II. Methods

### II.A. Experimental Setup

Figure 1 shows a schematic of the experimental channel investigated at ITLR as described in more detail by Vellaramkalayil et al.<sup>4</sup> It consists of four segments: The first two segments are fixed at opening angles of  $0^\circ$  and  $1^\circ$ , the last two segments are variable. For the present work the opening angle of these segments is set to  $2^\circ$ . The channel width is constant at  $B = 40$  mm, while the height inside the first segment is  $H = 35.4$  mm. Different Mach numbers between  $M = 1.7$  and  $M = 2.5$  can be realized by exchanging the Laval nozzle insert at the channel inlet. For the present study Mach numbers of 2.0 and 2.5 are investigated. The corresponding critical cross section heights  $H_i$  are listed in table 2. Since the channel is used as a model supersonic combustion chamber it contains two fuel injection stages: A lobed strut injector<sup>2,6</sup> serving as first stage and a wall ramp configuration used as second injection stage. These elements are included for all three-dimensional simulations of the present work in order to maintain complete comparability to the available experimental data. For the two-dimensional investigations the geometry is simplified by flattening the central injector due to symmetry considerations. In addition the second injection stage is omitted, as the influence on the flow field is considered to be negligible.

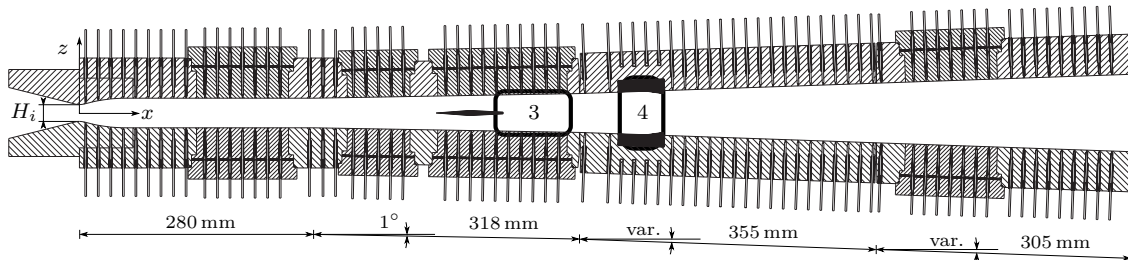


Figure 1. Schematic of the experimental channel at ITLR

A total of 128 static pressure measurement taps are arranged in the symmetry plane along the top and bottom walls of the channel. Total pressure, total temperature and mass flux are measured upstream of the Laval nozzle, thereby providing the inlet conditions for the numerical simulations. Optical access for Schlieren imaging can be realized using quartz windows at the locations 3 and 4 as indicated in figure 1. For all important channel features the detailed axial positions downstream of the critical Laval nozzle cross section are listed in table 1.

**Table 1. Axial positions of channel features**

Feature	Start	End
Strut injector	427.0 mm	513.0 mm
Window 3	500.0 mm	585.0 mm
Window 4	648.5 mm	695.5 mm
Wall ramp injectors	676.5 mm	698.0 mm

Schlieren images are obtained using a conventional Schlieren setup containing two lenses with a focal length of  $f = 100$  mm each. A high power light emitting diode serves as light source and a pinhole Schlieren edge is installed to capture flow density gradients along both  $x$  and  $z$  axis.

## II.B. Numerical Methods

When computing compressible high-speed flow, density based solvers proved to be superior to ones using a pressure based correction method because of the ability to predict shocks more accurately.<sup>7</sup> Therefore we implemented a new explicit, density based solver into the OpenFOAM environment as described by Makowka et al.<sup>8</sup> It is based on the discretization schemes developed by Kurganov and Tadmor<sup>9</sup> and includes support of multi-species transport and chemical reactions. For energy conservation the transport of total internal energy is used rather than transporting enthalpy in order to minimize pressure influence in the density based approach. Thermophysical properties are provided by JANAF-polynomials.<sup>10</sup> These polynomials have been slightly modified using the method developed by McBride and Gordon<sup>11</sup> to be valid down to  $T = 50$  K in order to account for the low static temperatures which may occur in supersonic flows.

Although the solver is transient by nature, a local time stepping scheme<sup>12</sup> has been implemented in order to speed up simulations for steady-state flows by introducing a local acoustic Courant number. In order to satisfy the Courant-Friedrichs-Lowy condition the local time step is calculated by

$$\Delta t = \Delta t(x) = \frac{\Delta x}{|u(x)| + c(x)} C_{max} \quad (1)$$

with the cell size  $\Delta x$ , the local flow velocity  $u(x)$  and the local speed of sound  $c(x)$ .

For the numerical simulations the experimental air flow conditions as listed in table 2 are used. In the experiments the copper channel is water-cooled, thus the channel walls are assumed to be isothermal at 400 K. Similarly, the central injector, which is cooled internally during experiments, is set to a constant wall temperature of 600 K. At the channel outlet a constant pressure of  $p = 96$  kPa is applied to account for the adaptation to ambient pressure in the experiments. For three-dimensional simulations a symmetry condition is defined at the channel center plane in order to reduce computational costs. Turbulence is modeled using the SST model,<sup>13</sup> which proved to be well suited for this type of flow in previous studies.<sup>3,4,14</sup> The flow turbulence level is set to 5 % and the ratio of turbulent to laminar viscosity is specified as  $\mu_t/\mu = 50$ . All calculations are conducted using second order accurate schemes in space and first order accuracy in time.

**Table 2. Inlet conditions for investigated cases**

$M$	$p_0$	$T_0$	$\dot{m}$	$H_i$
2.0	0.4 MPa	390 K	0.645 kg/s	20.12 mm
2.0	0.4 MPa	1300 K	0.353 kg/s	20.12 mm
2.5	0.6 MPa	390 K	0.581 kg/s	12.08 mm
2.5	0.6 MPa	1300 K	0.318 kg/s	12.08 mm

For comparison to experimental Schlieren imaging data (see section III.C) cold flow conditions at  $T_0 = 390\text{ K}$  are used. High temperature flow conditions at  $T_0 = 1300\text{ K}$  are employed for a more detailed investigation of the flow field and a comparison to both experimental pressure measurements and to numerical simulations obtained with a commercial CFD code.

The three-dimensional numerical setup is shown in more detail in figure 2. The channel side wall has been blanked for reasons of clarity. The cross sections at  $x = 0.4\text{ m}$  and  $x = 0.6\text{ m}$  are used for a comparison of numerical flow profiles (see sections III.A and III.B). For two-dimensional simulations the channel side wall and the symmetry plane are collapsed.

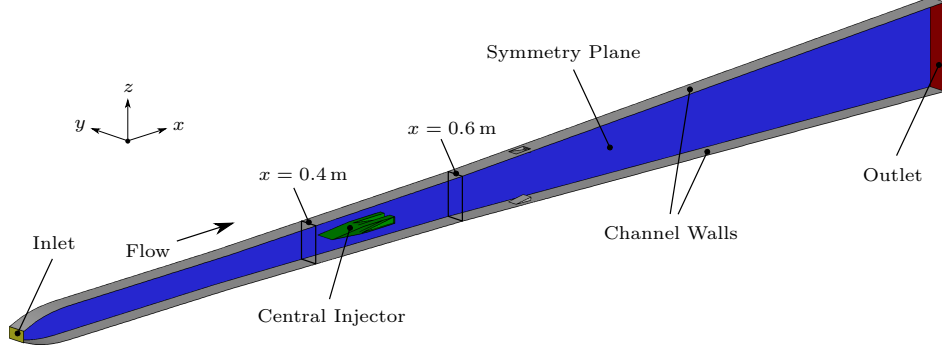


**Figure 2. Numerical setup**

Different wall treatment approaches are investigated using the two-dimensional setup. Besides the standard wall functions included in OpenFOAM also an enhanced compressible wall function employing a van-Driest transformation,<sup>15</sup> as reviewed by White<sup>16</sup> and by Smits and Dussauge,<sup>17</sup> has been implemented. According to van Driest

$$\frac{\partial u}{\partial y} = \frac{u_\tau}{\kappa y} \sqrt{\frac{T}{T_w}} \quad (2)$$

is valid, as the pressure in wall normal direction is constant for a perfect gas. Using

$$\frac{T}{T_w} = 1 + \left( \frac{T_r}{T_w} - 1 \right) \frac{u}{u_e} - r \frac{\gamma - 1}{2} M_e^2 \frac{T_e}{T_w} \left( \frac{u}{u_e} \right)^2 \quad (3)$$

for Prandtl number unity, which is approximately true for air flow, to substitute for the temperature ratio in equation (2) one obtains the van Driest effective velocity

$$u_{eq} = \int_{u_l}^u \sqrt{\frac{T_w}{T}} du = \frac{u_e}{b} \sin^{-1} \left( \frac{2b^2(u/u_e) - a}{\sqrt{a^2 + 4b^2}} \right) + \frac{u_e}{b} \sin^{-1} \left( \frac{a}{\sqrt{a^2 + 4b^2}} \right), \quad (4)$$

where

$$a = \left( 1 + r \frac{\gamma - 1}{2} M_e^2 \right) \frac{T_e}{T_w} - 1 \quad (5)$$

and

$$b^2 = r \frac{\gamma - 1}{2} M_e^2 \frac{T_e}{T_w}. \quad (6)$$

Here the subscript  $l$  represents a boundary condition at the lower end of the log law range. This effective velocity  $u_{eq}$  is then used to calculate the law of the wall for the turbulent viscosity  $\mu_t$ .

For all simulations which use wall functions the dimensionless wall distance

$$y_1^+ = \frac{u_\tau y}{\nu} \quad (7)$$

of the first cell at the wall is within the range of  $30 < y_1^+ < 60$ . The results are then compared to simulations using a finely resolved grid of  $y_1^+ \leq 1$  without the use of wall functions at the channel walls and at the injector. Due to limited computational resources three-dimensional simulations were only conducted with the wall function setup. However, as the main focus of these calculations is the validation of the highly

three-dimensional flow field inside the channel downstream of the strut injector this approach is shown to be sufficient.

A complete overview of all conducted simulations and their setup codes is given in table 3. To obtain the reference data of the commercial CFD code, a configuration with wall functions is used. Inlet conditions, grid and numerical settings are identical to the respective OpenFOAM simulations A1, B1, C and D.

**Table 3. Overview of conducted simulations**

$T_0$	$y_1^+$	Wall function	2D		3D	
			$M = 2.0$	$M = 2.5$	$M = 2.0$	$M = 2.5$
390 K	$30 < y_1^+ < 60$	OpenFOAM	-	-	CS	DS
1300 K	$30 < y_1^+ < 60$	OpenFOAM	A1	B1	C	D
1300 K	$30 < y_1^+ < 60$	van Driest	A2	B2	-	-
1300 K	$y_1^+ \leq 1$	-	A3	B3	-	-

### III. Results

#### III.A. Two-dimensional simulations

In order to verify the general functionality of the new solver a two-dimensional setup is chosen. In addition to a slightly simplified geometry and thus less complex flow field this approach also allows the reduction of computational costs due to the considerably smaller number of numerical grid cells compared to three-dimensional calculations as presented in section III.B.

Figure 3 shows the static wall pressure compared both to experimental data and to numerical simulations conducted with a commercial code. Note that for the case of  $M = 2.5$  the bottom wall pressure of the OpenFOAM simulation is displayed instead of the top wall pressure. The channel exit shock train tends to incline either to the top or bottom wall, although in the two-dimensional simulations the channel flow should theoretically be fully symmetric to the  $x$ -axis due to the flattened geometry of the injector. The same behavior is observed in the experiments, though for a three-dimensional injector. While in the experimental studies the shock train inclination is caused by small irregularities in the geometry of the combustor, in the numerical simulations the inclination direction appears to be random and is probably due to numerical uncertainties. However, this only affects the end of the channel downstream of  $x = 0.7\text{ m}$  and not the investigated cross-sections more upstream.

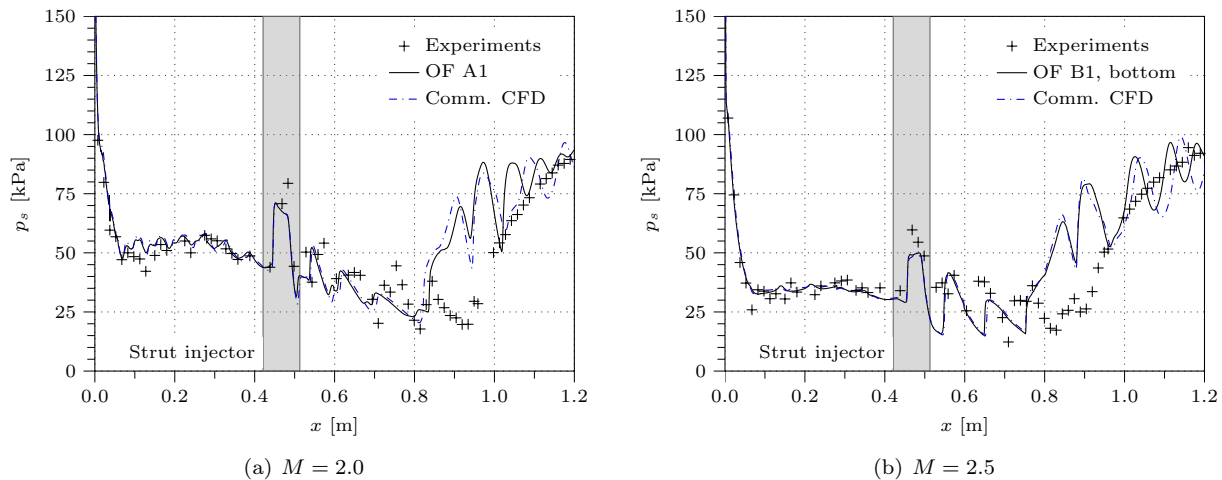


**Figure 3. Wall pressure distribution, 2D**

For  $x \leq 0.7\text{ m}$  a very good agreement of both numerical codes is found. Also the experimental measurements are well reproduced in this region. The shocks originating at the injector and their reflections at the walls are predicted with reasonable accuracy. However, due to the flattened geometry of the injector the

corresponding effects on experimental pressure data are not matched precisely. The onset of the channel exit shock train differs slightly between the two CFD codes. However, as according to experimental tests the shock train is a highly transient phenomenon, deviations when using a steady state numerical approach and a two-equation eddy viscosity model are to be expected.

The comparison of flow profiles at  $x = 0.4\text{ m}$  and  $x = 0.6\text{ m}$  for  $M = 2.0$  is shown in figure 4. Both temperature and velocity profiles are investigated. For an undisturbed channel flow upstream of the injector regarding the velocity profile reasonable agreement between the codes is achieved. Considering the temperature profile the usage of wall functions within OpenFOAM results in a higher temperature gradient directly at the channel walls. Employing the enhanced wall function including a van-Driest transformation does not change the temperature gradient near the walls. However, in the central region of the channel the temperature and velocity profiles are in better agreement to the results of the commercial code. When avoiding wall functions by applying a finer mesh with  $y_1^+ \leq 1$  OpenFOAM tends to match the commercial code, which uses wall functions, better near the walls. For both investigated Mach numbers the core flow temperature upstream of the injector is slightly lower for OpenFOAM when resolving the walls.

As presumed the flow field upstream of the channel exit shock train proves to be completely symmetrical, thus the influence of the different shock train inclination direction between the two codes can be neglected.

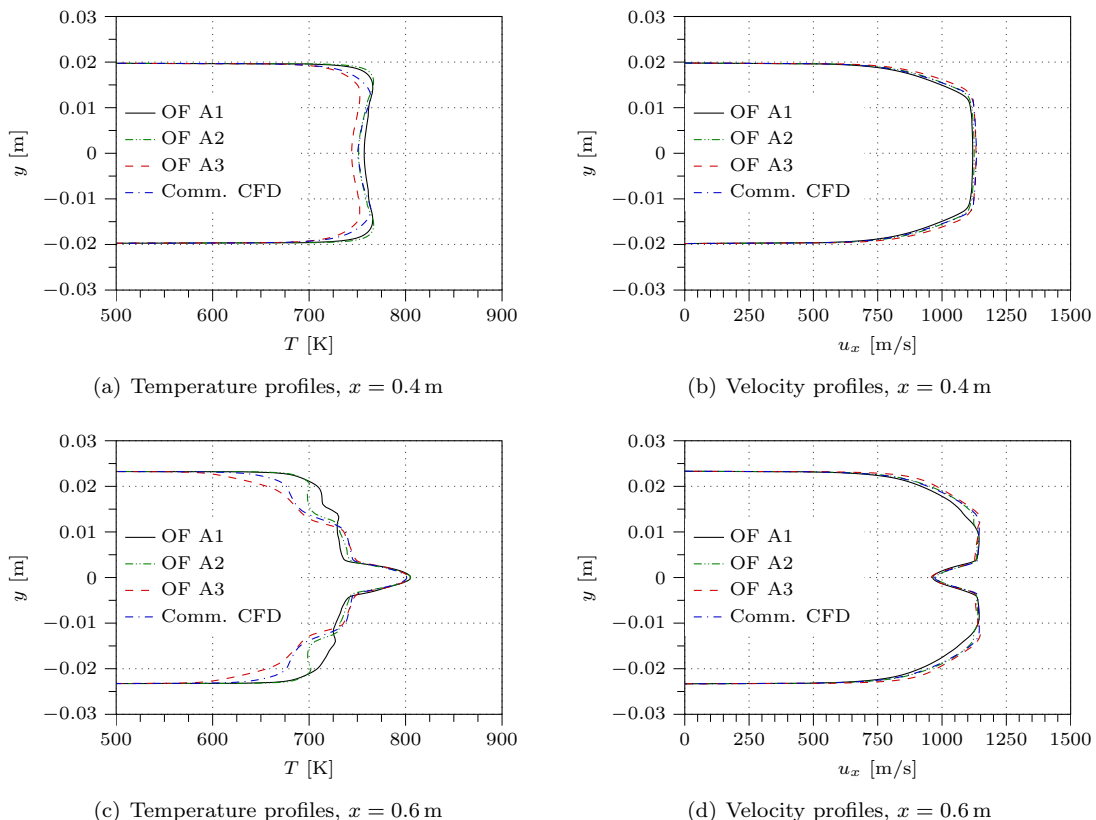


**Figure 4.** Flow profiles,  $M = 2.0$ , 2D

A comparable behavior is observed for the position further downstream at  $x = 0.6\text{ m}$ . The influence of the injector on the flow field is clearly visible, shock waves originating at the injector are reflected at the top and bottom walls and are crossing the flow field. Combined with the wake of the injector itself, regions with lower velocity and thus higher static temperature develop in the center of the channel. Again, the simulation without wall functions yields more similar results to the commercial code especially regarding the temperature profile near the channel walls.

At  $M = 2.5$  the behavior is similar as shown in figure 5. The effect of the higher Mach number on the temperature profiles is predicted correctly by both codes, as now the static temperatures within the core flow is lower than the temperature in the vicinity of the walls.

For this Mach number setup B1 again predicts a rise in static temperature in the wake of the injector, while the commercial code and the finer resolved simulation of setup B3 do not. This is due to a slightly

different position of the reflected compression shocks. For setup B1 the cross-section at  $x = 0.6$  m is directly downstream of a shock intersection in the channel center thus causing a higher static temperature and a lower flow velocity. In contrast, for setup B3 the shock intersection is located slightly downstream of  $x = 0.6$  m.

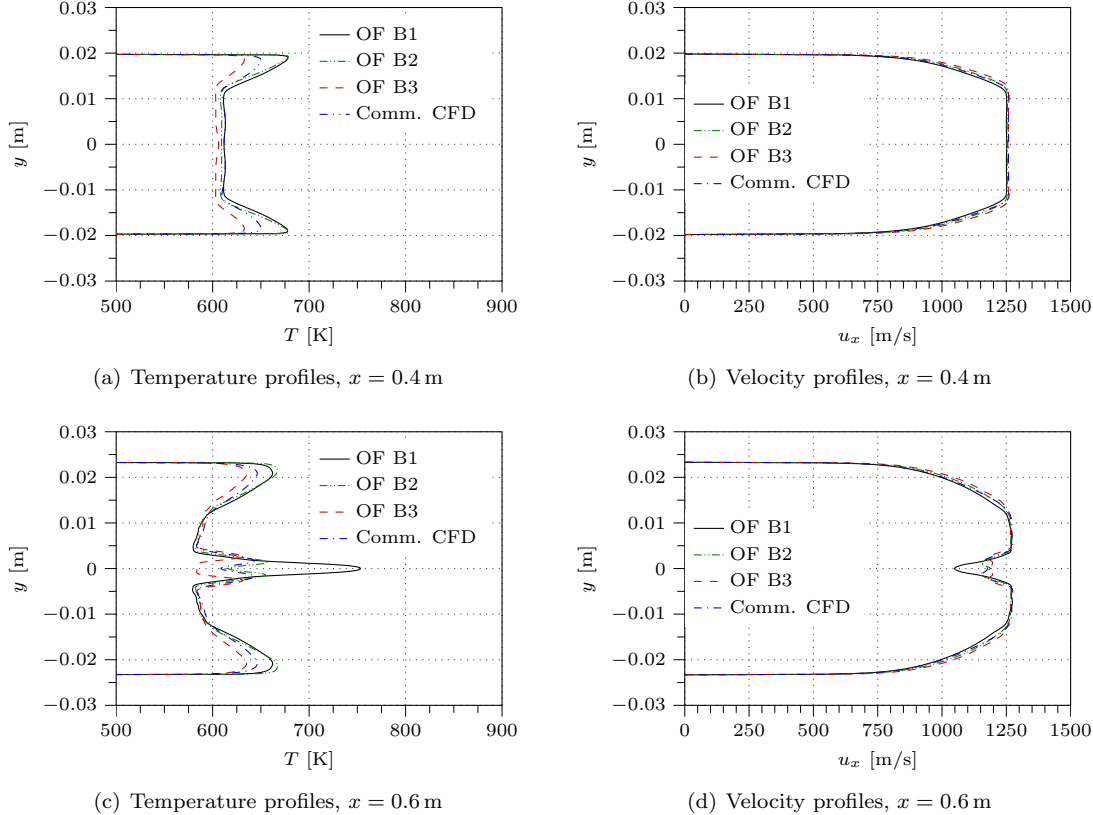


**Figure 5.** Flow profiles,  $M = 2.5$ , 2D

When applying the enhanced wall functions of setup B2 only small deviations to the conventional setup B1 can be observed at  $x = 0.4$  m. Further downstream at the second investigated cross section setup B2 produces considerably better results, since here the shock system position in the center of the channel fits better to the commercial code and to the wall resolved simulation B3. However, the overpredicted temperature gradient at the wall is not influenced by the change of the wall function type.

### III.B. Three-dimensional simulations

Three-dimensional computations were conducted using the standard wall function setup only due to the increasing computational costs when applying advanced wall treatment or finer grids. Figure 6 shows the static wall pressure at the top wall compared to the experimental data and to the commercial code. In contrast to the two-dimensional simulations, for  $M = 2.0$  the injector leading edge shock is overpredicted. This is due to the formation of a separation region at the impact of the leading edge shock onto the channel wall, which then expands upstream up to  $x = 0.4$  m. However, the flow reaccelerates and matches the experimental and numerical data again downstream of the injector. This behavior is unique for the lower Mach number, for  $M = 2.5$  upstream of the strut injector good agreement is obtained.

Our OpenFOAM code tends to predict the onset point of the shock train further downstream compared to the commercial code. For  $M = 2.0$  the results match the experimental data up to  $x = 0.8$  m, whereas for  $M = 2.5$  the numerical shock train onset nearly matches the experimental data. For both investigated Mach numbers the commercial code places the beginning of the shock train around 50 mm to 100 mm more upstream depending on the inflow Mach number.

Just as for the two-dimensional simulations two cross-sections at  $x = 0.4$  m and  $x = 0.6$  m are investigated in more detail. The results for  $M = 2.0$  are presented in figure 7. Here the data contours obtained with OpenFOAM are depicted on the left side of each subfigure, while the corresponding right sides show the

numerical results of the commercial code. The symmetry plane is located at the respective right hand side of each contour plot.

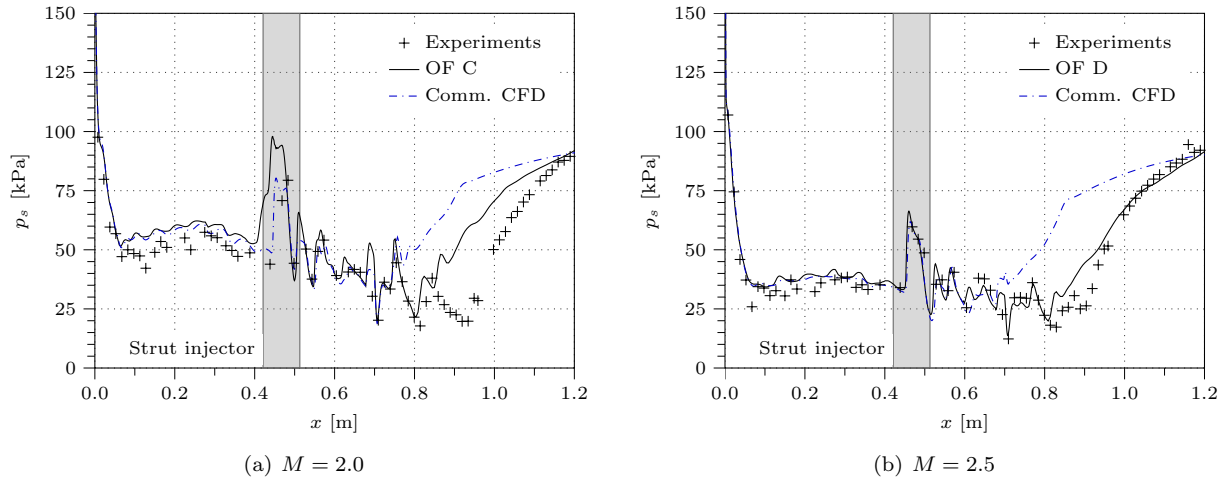


**Figure 6. Wall pressure distribution, 3D**

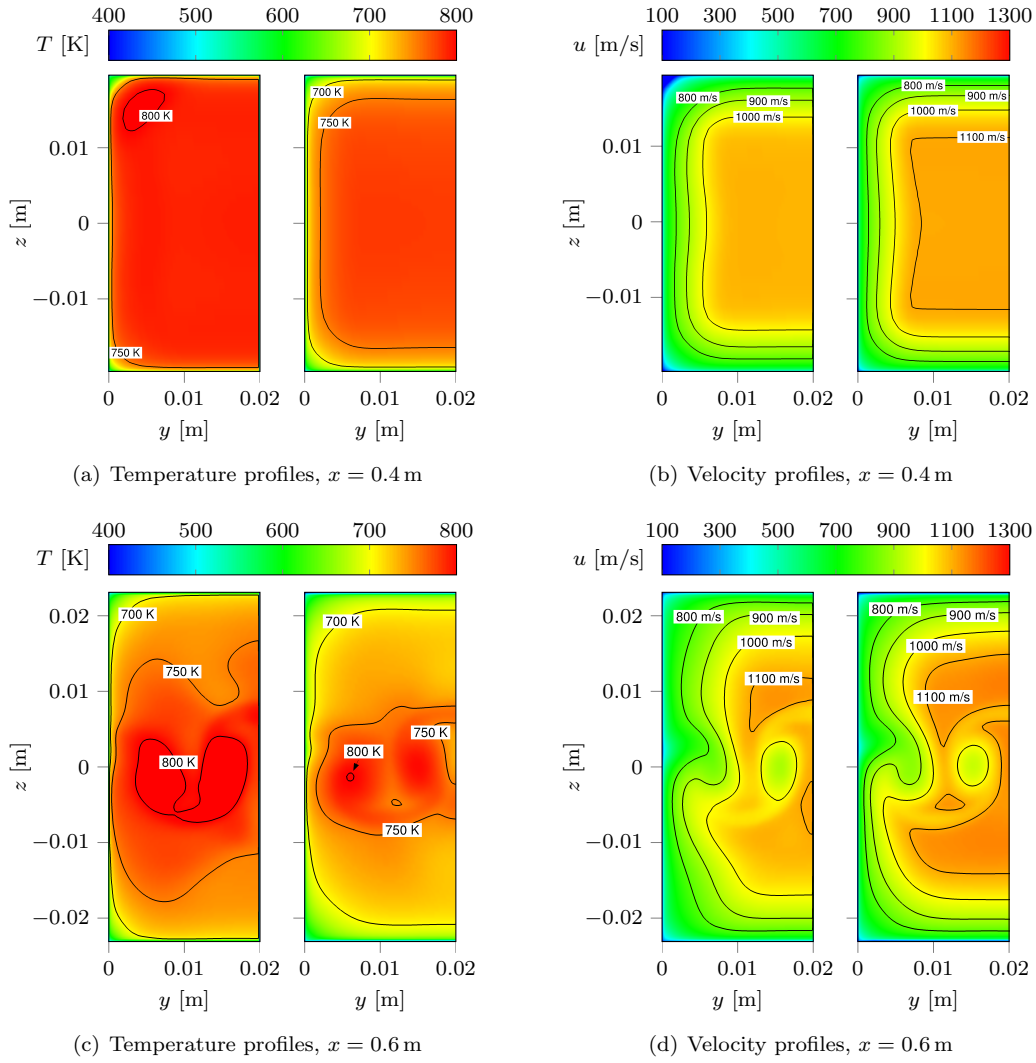


**Figure 7. Flow profiles,  $M = 2.0$ , 3D (left: OpenFOAM, right: Commercial code)**

As already observed when evaluating the wall pressure distribution, in the plane at  $x = 0.4\text{ m}$  subsonic regions form in the channel corners, thus confirming the beginning of flow separation. In this region the static temperature is considerably increased in contrast to the remainder of the channel cross section. Compared to the commercial code OpenFOAM predicts a slightly lower velocity for the whole cross section, resulting in a somewhat higher static temperature level.

The same phenomenon is observed for the second cross section at  $x = 0.6\text{ m}$ . Here the flow disturbances due to the wake of the strut injector can be seen, which are characterized by the stream-wise vortices in both temperature and velocity distributions. The temperature level continues to be slightly increased for OpenFOAM, while the vortex shape is correctly simulated.

Figure 8 presents the results for  $M = 2.5$ . Considering the undisturbed channel flow the velocity profile is similar to the one predicted by the commercial code. As seen in figure 8(a) the temperature in the vicinity of the channel walls is considerably higher for OpenFOAM, which is in accordance with the two-dimensional computations. At  $x = 0.6\text{ m}$  the characteristic wake of the injector is visible again, the shape is similar to the results for  $M = 2.0$ . While the velocity profile is a good match, again OpenFOAM tends to predict a slightly higher temperature in the wake in addition to the deviations near the wall.

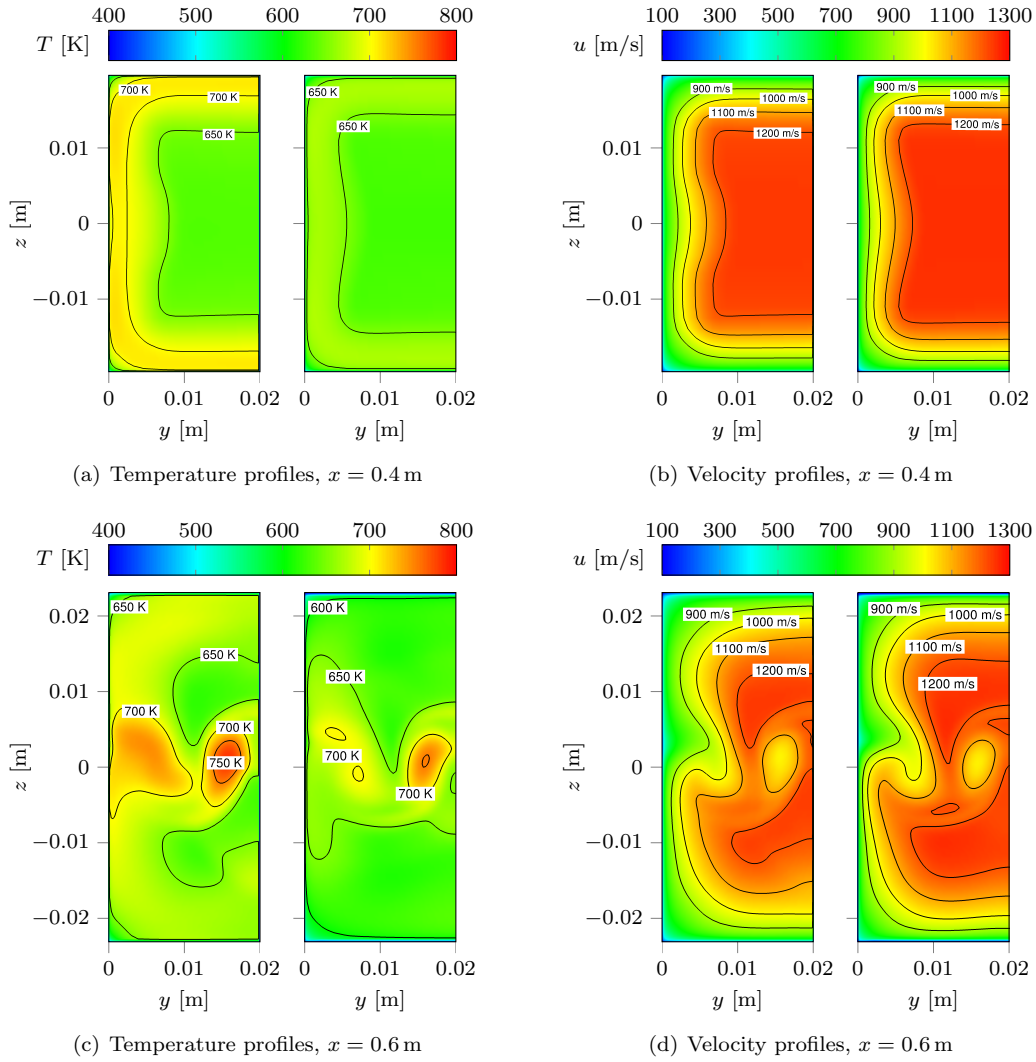


**Figure 8. Flow profiles,  $M = 2.5$ , 3D (left: OpenFOAM, right: Commercial code)**

When comparing the different Mach numbers to each other the general flow field features are identical: High temperature regions are developing downstream of the trailing edge of the injector, caused by both the shock system generated at the injector and by the lobed shape of the injector itself. The shape of the vortices is similar, though the swirl is more pronounced for the higher Mach number. This leads to the

conclusion that in spite of the differences in temperature due to wall modeling the key flow features are predicted correctly by both codes. Especially regarding flow velocity good agreement is obtained.

### III.C. Comparison to Schlieren imaging

Schlieren images of the channel flow were obtained at a total temperature of  $T_0 = 390\text{ K}$  using the simulation setups CS and DS. For high flow temperatures as investigated in the previous sections the high temperature gradients at the quartz windows render conventional Schlieren imaging impossible. As the total flow pressure is kept constant compared to the hot gas simulations, the lower temperature results in higher air mass flows as stated above in table 2.

Figures 9 and 10 show the comparison of experimental and numerical Schlieren data for both investigated Mach numbers. As the main shock system inside the channel is nearly symmetrical with respect to the  $x$ - $z$ -plane, only the upper channel half is shown in the experimental Schlieren images. The lower halves of the figures display the mirrored numerical Schlieren results for the same channel half side. The trailing edge of the strut injector is visible on the left hand side of the first window, the leading edges of the second stage ramp injectors can be seen at the top and bottom channel walls on the right hand side of the second window. The distinct flow features are captured by the numerical simulations: The oblique shock and expansion system in the wake of the strut injector, which is created by the lobed structure of the injector, is reproduced correctly. Also the bow shock, which forms at the leading edge of the wall ramps, is simulated with the correct inclination angle.

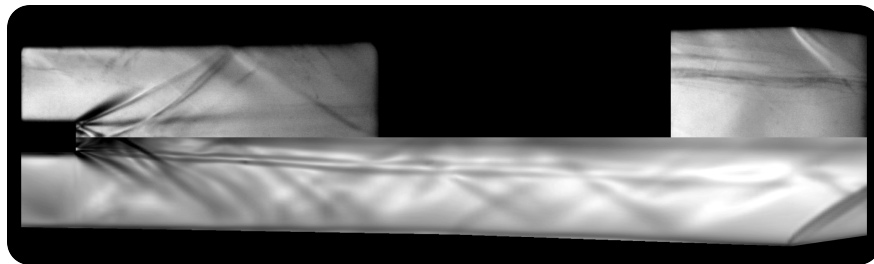


**Figure 9.** Comparison of experimental (top) and numerical (bottom) Schlieren images,  $M = 2.0$

When comparing the results for both Mach numbers the reduction of the shock inclination angles due to the higher flow velocity is clearly visible in both experimental and numerical data. The shock system in the wake of the injector is stretched axially, also the shock impact locations at the channel walls are shifted downstream. The bow shock at the ramps inclines considerably stronger towards the wall for the higher Mach number of  $M = 2.5$ .

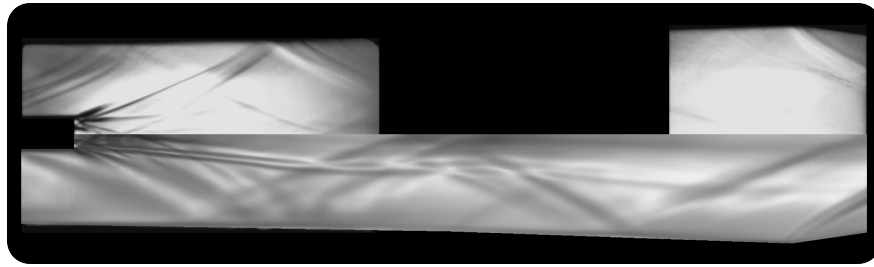


**Figure 10.** Comparison of experimental (top) and numerical (bottom) Schlieren images,  $M = 2.5$

## IV. Conclusion

In the presented study a supersonic hot air flow has been numerically investigated using a newly created supersonic solver within the CFD software package OpenFOAM. Both two-dimensional and three-dimensional simulations were carried out. Experimental reference measurements were obtained, also numerical results by a commercial code have been used for comparison. The evaluation of the two-dimensional simulations yielded that the new solver is able to produce good results. The experimental data were well

reproduced and flow profiles were comparable to those predicted by the commercial code. A detailed investigation of different wall treatment approaches showed that a wall resolution of  $y_1^+$  is desirable, but highly disadvantageous regarding computational costs. When using wall functions for supersonic flows in OpenFOAM, an enhanced approach containing a van-Driest transformation produced better results compared to the standard set of wall functions included in OpenFOAM. However, both wall functions currently lack accuracy when predicting the temperature gradient in the vicinity of the wall for supersonic conditions.

Three-dimensional simulations confirmed that the new solver is also able to predict the complex flow field in the wake of the strut injector correctly. Again, due to the use of wall functions the temperature gradient was overpredicted at the wall compared to the commercial code. However, the core flow temperature was predicted similarly by both CFD codes. In addition to the hot gas flow also cold flow conditions were investigated and compared to experimentally obtained Schlieren images. It was verified that the numerical simulations are able to predict the shock system inside the channel correctly. Therefore we showed that the new solver is able to accurately simulate non-reacting supersonic channel flows. Future studies will include the further expansion of the new solver as well as the implementation of a more sophisticated temperature wall function for supersonic flows.

## Acknowledgments

This work has been carried out within the Graduate School ‘Aero-Thermodynamic Design of a Scramjet Propulsion System for Future Space Transport Vehicles (GRK1095/2)’. The authors would like to thank the German Research Foundation (Deutsche Forschungsgemeinschaft) for their support. Furthermore we greatly acknowledge the High Performance Computing Center Stuttgart (HLRS) for support and supply of computational time on the Cray XE6 platform under grant number 12995.

## References

- <sup>1</sup>Jasak, H., Jemcov, A., and Tukovic, Z., “OpenFOAM: A C++ Library for Complex Physics Simulations,” *International Workshop on Coupled Methods in Numerical Dynamics*, 2007.
- <sup>2</sup>Vellaramkalayil, J. J., Scheuermann, T., and von Wolfersdorf, J., “Numerical and Experimental Investigation of a Two-Staged Supersonic Combustion Chamber,” *16th AIAA/DLR/DGLR International Space Planes and Hypersonic Systems and Technologies Conference*, 2009.
- <sup>3</sup>Vellaramkalayil, J. J., Scheuermann, T., Winkler, S., von Wolfersdorf, J., and Banica, M. C., “Experimental and Numerical Study of a Supersonic Combustion Chamber with different Two-Staged Injection Concepts,” *46th AIAA/ASME/SAE/ASEE Joint Propulsion Conference & Exhibit and 8th Annual International Energy Conversion Engineering Conference*, 2010.
- <sup>4</sup>Vellaramkalayil, J. J., Scheuermann, T., and von Wolfersdorf, J., “Analysis of a Two-Staged Supersonic Combustion Chamber using Experiments and Simulations,” *17th AIAA International Space Planes and Hypersonic Systems and Technologies Conference*, 2011.
- <sup>5</sup>Scheuermann, T., Chun, J., and von Wolfersdorf, J., “Experimental Investigations of Scramjet Combustor Characteristics,” *15th AIAA International Space Planes and Hypersonic Systems and Technologies Conference*, 2008.
- <sup>6</sup>Gerlinger, P., Schneider, F., and Aigner, M., “Numerical Investigation of Mixing Enhancement by Streamwise Vorticity in Supersonic Combustors,” *17th International Symposium on Air Breathing Engines*, 2005.
- <sup>7</sup>Ettner, F. A., *Effiziente numerische Simulation des Deflagrations-Detonations-Übergangs*, Ph.D. thesis, Lehrstuhl für Thermodynamik, Technische Universität München, 2013.
- <sup>8</sup>Makowka, K., Gurtner, M., Paukner, D., Sattelmayer, T., and Kau, H. P., “Numerical and Experimental Investigation of a Central Strut Injector with Perpendicular Injection for Scramjet Applications,” *5th European Conference for Aeronautic and Space Sciences*, 2013.
- <sup>9</sup>Kurganov, A. and Tadmor, E., “New High-Resolution Central Schemes for Nonlinear Conservation Laws and Convection-Diffusion Equations,” *Journal of Computational Physics*, Vol. 260, 2000, pp. 241–262.
- <sup>10</sup>Chase Jr., M. W., Davies, J., Downey Jr., J. R., Frurip, D. J., McDonald, R. A., and Syverud, A. N., “JANAF Thermochemical Tables,” *Journal of Physical and Chemical Reference Data*, Vol. 14, Supplement No.1, 1985.
- <sup>11</sup>McBride, B. J. and Gordon, S., “Computer Program for Calculating and Fitting Thermodynamic Functions,” Tech. Rep. NASA Reference Publication 1271, National Aeronautics and Space Administration, 1992.
- <sup>12</sup>Anderson Jr., J. D., *Computational Fluid Dynamics*, McGraw Hill, Inc., 1995.
- <sup>13</sup>Menter, F. R., Kuntz, M., and Langtry, R. B., “Ten Years of Industrial Experience with the SST Turbulence Model,” *Turbulence, Heat and Mass Transfer IV*, 2003.
- <sup>14</sup>Banica, M., Scheuermann, T., Chun, J., Weigand, B., and von Wolfersdorf, J., “Numerical Study of Supersonic Combustion Processes with Central Strut Injection,” *Journal of Propulsion and Power*, Vol. 26, No. 4, 2010.
- <sup>15</sup>van Driest, E. R., “Turbulent Boundary Layer in Compressible Fluids,” *Journal of the Aeronautical Sciences*, Vol. 18, 1951, pp. 145–160.
- <sup>16</sup>White, F. M., *Viscous Fluid Flow*, McGraw Hill, Inc., 3rd ed., 2006.
- <sup>17</sup>Smits, A. J. and Dussauge, J.-P., *Turbulent Shear Layers in Supersonic Flow*, Springer-Verlag, 2nd ed., 2006.